10.1098/rsta.2004.1405

THE ROYAL SOCIETY

Hybrid computations with flux exchange

By G. Wagner[1] and E. G. Flekkøy[2]

[1]*Department of Engineering, Haugesund Engineering College, 5528 Haugesund, Norway*
[2]*Department of Physics, University of Oslo, PB1048 Blindern, 0316 Oslo, Norway* (e.g.flekkoy@fys.uio.no)

Published online 2 June 2004

We discuss a hybrid scheme that is based on flux exchange between a particle and a continuum system which reside in two slightly overlapping volumes in space. The scheme ensures conservation of mass, momentum and energy between a system of Lennard-Jones particles and a continuum description given by the compressible Navier–Stokes equations. An implementation in two dimensions employing the compressible Navier–Stokes equations to describe the continuum, and the Lennard-Jones potential to describe the particles, is discussed. The accuracy of the coupling scheme is tested successfully for the case of homogeneous flow and discussed for the more general case.

Keywords: hybrid models; multi-scale computation; hydrodynamics

1. Introduction

In many physical systems, such as those of a moving contact line, fracture or sliding friction, nanoscale processes couple directly to the large-scale dynamics.

From a computational point of view the challenge is to deal with the many scales involved. An observation that will make this possible in a number of situations is that the small-scale dynamics need only be resolved in a very small spatial area, whereas the bulk dynamics is adequately described by coarse-scale continuum dynamics. The design of such multiscale hybrid schemes, as is discussed in the present paper, relies on this observation. The present hybrid scheme couples a local, small-scale particle description to a large-scale continuum description. This is done in a hydrodynamic setting where the particles are governed by a Lennard-Jones potential and the continuum by the Navier–Stokes equations.

In recent works hybrid descriptions have been applied in the context of fracture (see Abraham *et al*. 1998; Rafii *et al*. 1998) as well as in hydrodynamics. Early hydrodynamic studies where suited to boundary flow problems but did not involve mass or energy exchange (see O'Connel & Thompson 1995; Hadjiconstantinou 1999*a*, *b*), and in some cases high-Mach-number flows, as is discussed by Garcia *et al*. (1999). In order to ensure conservation of mass and momentum, an explicit flux-exchange scheme was introduced that would also work in dense liquid systems (Flekkøy *et al*.

One contribution of 21 to a Theme 'Connecting scales: micro, meso and macro processes'.

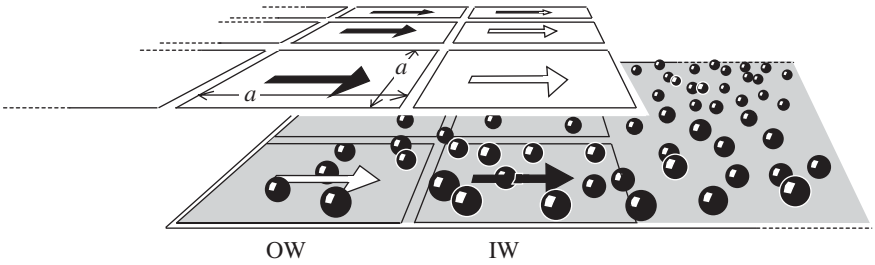

Figure 1. Illustration of the overlap region consisting of an IW section and an OW section. Full arrows represent flux measurements, open arrows fluxes that are imposed. The lattice spacing of the continuum solver is denoted a.

2000). This scheme was later expanded to include energy flux exchange by Wagner *et al*. (2002) and by Delgado-Buscalioni & Coveney (2003).

The purpose of the present paper is partly to expand upon the work reported by Wagner *et al*. (2002) and partly to discuss some of the basic characteristics and limitations of the flux-exchange scheme, in particular when energy is exchanged along with mass and momentum. For this purpose test simulations are carried out. These simulations show that, while all quantities (mass, momentum and energy) are conserved to relative order 10^{-4} in homogeneous flow simulations, the accuracy drops once gradients are introduced.

2. Coupling scheme and its implementation

The continuum describing mass, momentum and energy flow is represented by a grid of nodes where the node spacing is chosen to be much larger than the microscopic length-scale. Conservation of mass, momentum and energy in the bulk of the particle and continuum simulations is guaranteed by design. The challenge is to make the coupling between the two systems conservative.

The coupling cannot consist in the mutual prescription of thermodynamic variables such as pressure, density, temperature, etc. Such a scheme would depend on the correctness of all transport coefficients and constitutive relations. A coupling scheme is physically sound and consistent only when the basic conservation laws do not depend on exact measurements of these relations. Remember that particle descriptions are needed in general where the continuum descriptions are no longer adequate.

The overlap region illustrated in figure 1 is composed of an 'inner wall' (IW) and an 'outer wall' (OW). At the IW, time-averaged particle fluxes are measured, while the continuum fluxes are obtained at the OW. The coupling consists in imposing, as boundary conditions on both systems, the *arithmetic mean* of the fluxes measured at the interface. The idea is to make the fluxes that exit one systems enter the other. This guarantees the desired conservation of mass, momentum and energy.

All fluxes can be computed on each of the nodes defining the continuum. The mass flux density $\boldsymbol{j}_\mathrm{c}$ is given by

$$\boldsymbol{j}_\mathrm{c} = \rho_\mathrm{c}\boldsymbol{u}_\mathrm{c}, \tag{2.1}$$

where ρ_c and $\boldsymbol{u}_\mathrm{c}$ denote the continuum mass density and velocity vector, respectively. The momentum flux density $\boldsymbol{\Pi}_\mathrm{c}$ is a tensor given by

$$\boldsymbol{\Pi}_\mathrm{c} = \rho_\mathrm{c}\boldsymbol{u}_\mathrm{c}\boldsymbol{u}_\mathrm{c} - \mu[\nabla\boldsymbol{u} + (\nabla\boldsymbol{u})^\mathrm{T} - \nabla\cdot\boldsymbol{u}] - \lambda\nabla\cdot\boldsymbol{u} + p\mathbf{1}, \tag{2.2}$$

where μ and λ are the dynamic and bulk viscosities respectively, p is the pressure, superscript 'T' denotes the transpose, and $\mathbf{1}$ is the unit tensor. The energy flux density $\boldsymbol{e}$ is given by

$$\boldsymbol{e}_{\mathrm{c}} = \rho_{\mathrm{c}}\boldsymbol{u}_{\mathrm{c}}\epsilon_{\mathrm{c}} + (\boldsymbol{\Pi}_{\mathrm{c}} - \rho_{\mathrm{c}}\boldsymbol{u}_{\mathrm{c}}\boldsymbol{u}_{\mathrm{c}}) \cdot \boldsymbol{u}_{\mathrm{c}} + \boldsymbol{q}_{\mathrm{c}}. \tag{2.3}$$

Here ϵ_{c} is the energy per unit mass and the heat flux is given by $\boldsymbol{q}_{\mathrm{c}} = -k\nabla T_{\mathrm{c}}$, where k and T_{c} denote the heat conductivity and the continuum temperature, respectively.

In the particle picture as described by Resibois & De Leener (1977), the mass flux density $\boldsymbol{j}_{\mathrm{p}}$ is defined as

$$\boldsymbol{j}_{\mathrm{p}} = \frac{1}{V}\sum_{i\in V} m_{\mathrm{p}}\boldsymbol{u}_{\mathrm{p}}^{i}, \tag{2.4}$$

where m_{p} and $\boldsymbol{u}_{\mathrm{p}}^{i}$ denotes the mass and velocity of the ith particle in $V = a^2$. The momentum flux tensor $\boldsymbol{\Pi}_{\mathrm{p}}^{(\alpha,\beta)}$ ($\alpha, \beta = x, y$ in two dimensions) is given by

$$\Pi_{\mathrm{p}}^{(\alpha\beta)} = \frac{1}{V}\left[\sum_{i\in V} m_{\mathrm{p}}u_{\mathrm{p}}^{i\alpha}u_{\mathrm{p}}^{i\beta} + \sum_{i\in V<j} r^{ij\beta}F^{ij\alpha}\right], \tag{2.5}$$

where $\boldsymbol{r}^{ij}$ is the position vector pointing from the ith to the jth particle,

$$F^{ij\alpha} = -\frac{\partial V_{\mathrm{LJ}}(r^{ij})}{\partial r^{ij\alpha}}$$

and V_{LJ} is an isotropic interparticle potential.

The particle energy flux density $\boldsymbol{e}_{\mathrm{p}}$ is given by

$$\boldsymbol{e}_{\mathrm{p}} = \frac{1}{V}\sum_{i\in V}\left[\boldsymbol{u}_{\mathrm{p}}^{i}\left(\frac{m_{\mathrm{p}}(\boldsymbol{u}_{\mathrm{p}}^{i})^2}{2} + \frac{1}{2}\sum_{ij\in V} V_{\mathrm{LJ}}(\boldsymbol{r}^{ij})\right) + \frac{1}{4}\sum_{ij\in V}\boldsymbol{F}^{ij}\cdot(\boldsymbol{u}_{\mathrm{p}}^{i} + \boldsymbol{u}_{\mathrm{p}}^{j})\boldsymbol{r}^{ij}\right]. \tag{2.6}$$

The particles propagate following Newton's equations of motion. In a typical cycle, the particle fluxes are time averaged in the IW section during a number N of molecular dynamics (MD) steps, each covering a time span δt. Then the mean of the particle fluxes in the IW section and of the continuum fluxes in the OW section is formed:

$$\langle\boldsymbol{j}\rangle = \frac{\boldsymbol{j}_{\mathrm{c}} + \boldsymbol{j}_{\mathrm{p}}}{2}, \qquad \langle\boldsymbol{\Pi}\rangle = \frac{\boldsymbol{\Pi}_{\mathrm{c}} + \boldsymbol{\Pi}_{\mathrm{p}}}{2}, \qquad \langle\boldsymbol{e}\rangle = \frac{\boldsymbol{e}_{\mathrm{c}} + \boldsymbol{e}_{\mathrm{p}}}{2}. \tag{2.7}$$

The continuum equations are then integrated forward in time, using a step of $\Delta t = N\delta t$. The Neumann boundary conditions for the integration are given by the normal components, relative to the interface, of the mean fluxes, $\langle\boldsymbol{j}\rangle\cdot\boldsymbol{n}$, $\langle\boldsymbol{\Pi}\rangle\cdot\boldsymbol{n}$ and $\langle\boldsymbol{e}\rangle\cdot\boldsymbol{n}$, where $\boldsymbol{n}$ denotes the unit vector normal to the interface. Now the next cycle of N MD steps follows, during which the fluxes $\langle\boldsymbol{j}\rangle\cdot\boldsymbol{n}$, $\langle\boldsymbol{\Pi}\rangle\cdot\boldsymbol{n}$ and $\langle\boldsymbol{e}\rangle\cdot\boldsymbol{n}$ are continuously imposed on the particle system. Integrated over a full cycle, the particles receive the same amount of flux that is taken out of the continuum, and vice versa. N should be chosen large for numerical efficiency; it is limited by the stability criteria of the algorithm chosen for the integration of the continuum equations.

3. Finite differencing of the continuum equations

To make the continuum description as close as possible to a description of the particle system, preliminary measurements of the particle system are carried out. The viscosity and the heat conductivity as well as the constitutive equations, $p_{\mathrm{p}} = p_{\mathrm{p}}(\rho_{\mathrm{p}}, T_{\mathrm{p}})$

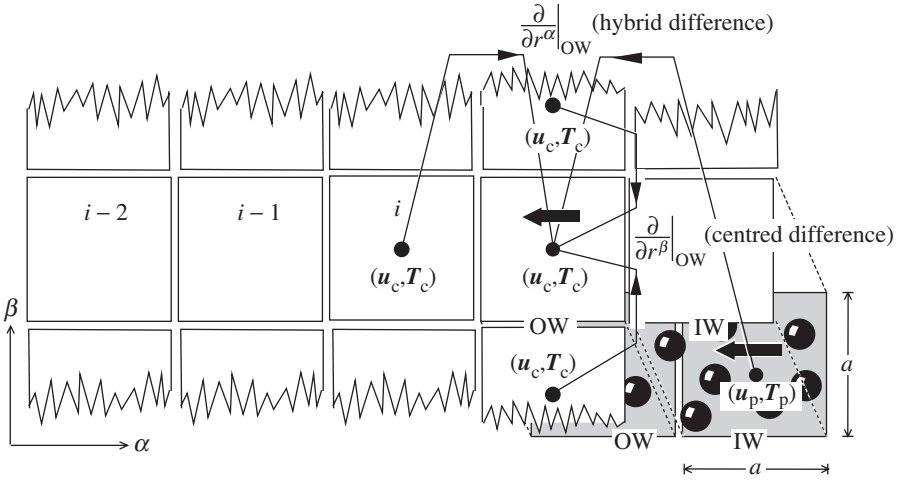

Figure 2. Illustration of how the *hybrid gradient* is evaluated.

and $T_\mathrm{p} = T_\mathrm{p}(\rho_\mathrm{p}, \epsilon_\mathrm{p})$, are determined. Here the subscript 'p' indicates that the quantities are measured in the particle system.

Using these measurements as well as $p_\mathrm{c} = p_\mathrm{c}(\rho_\mathrm{c}, T_\mathrm{c})$ and $T_\mathrm{c} = T_\mathrm{c}(\rho_\mathrm{c}, \epsilon_\mathrm{c})$, where the subscript 'c' now indicates continuum values, the set of continuum equations takes the standard form

$$\frac{\partial \rho_\mathrm{c}}{\partial t} + \nabla \cdot \boldsymbol{j}_\mathrm{c} = 0, \tag{3.1}$$

$$\frac{\partial \rho_\mathrm{c} \boldsymbol{u}_\mathrm{c}}{\partial t} + \nabla \cdot \boldsymbol{\Pi}_\mathrm{c} = 0, \tag{3.2}$$

$$\frac{\partial \rho_\mathrm{c} \epsilon_\mathrm{c}}{\partial t} + \nabla \cdot \boldsymbol{e}_\mathrm{c} = 0. \tag{3.3}$$

For simplicity it is assumed that the bulk viscosity $\lambda = \frac{2}{3}\mu$. Central differences across neighbouring nodes are used to evaluate derivatives. For instance, the derivative of the mass flux component j_c^α takes the form

$$\left.\frac{\partial j_\mathrm{c}^\alpha}{\partial r^\beta}\right|_i \approx \frac{j_\mathrm{c}^{(i+1)\alpha} - j_\mathrm{c}^{(i-1)\alpha}}{2a}, \tag{3.4}$$

where i runs in the β direction. Central differencing (as opposed to forward or backward differencing) is important if fluxes are to be imposed on more than one boundary of the continuum domain. Anisotropic differencing would imply an unequal treatment of the boundaries.

(*a*) *Hybrid gradients*

The continuum flux densities $\boldsymbol{j}_\mathrm{c}$, $\boldsymbol{\Pi}_\mathrm{c}$ and $\boldsymbol{e}_\mathrm{c}$ must be evaluated on each node in the OW section, according to equations (2.1)–(2.3). This means that the derivatives of mass density, velocity and temperature must be evaluated. Regular central differencing cannot be used, as the continuum values on the IW nodes are imposed by the flux boundaries and thus are not valid to provide flux estimates. Instead, the

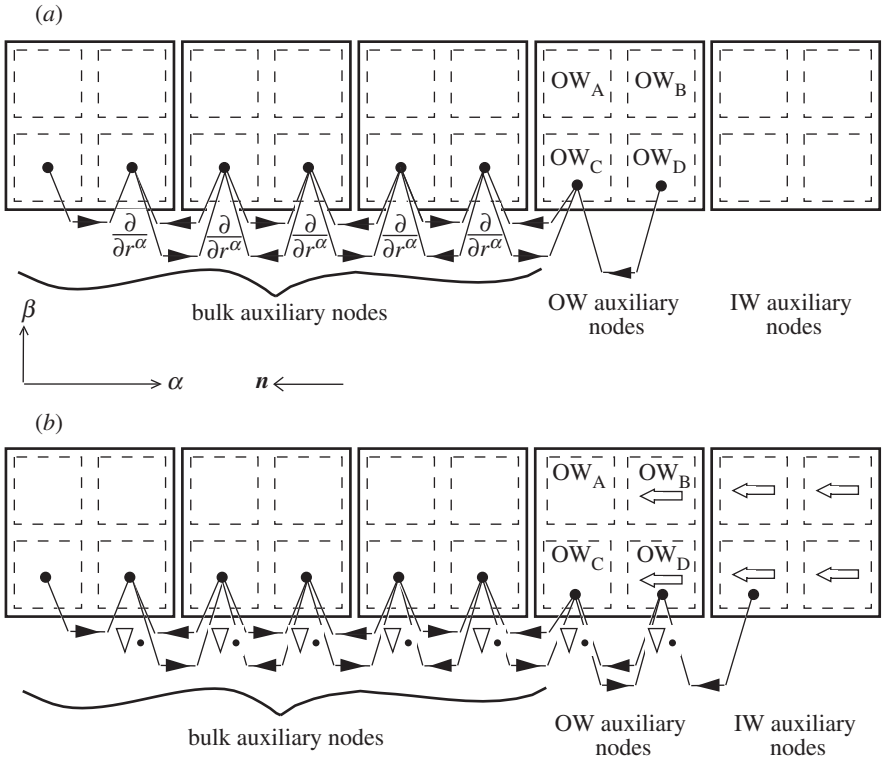

Figure 3. The flux computation and flux derivation used in the integration of the continuum equations. (*a*) The derivatives used in the flux computation were approximated using centred differencing (arrows). (*b*) Open arrows show flux values that were inserted.

derivatives involved in the flux computation are estimated using a *hybrid gradient*. This gradient is found by substituting particle data for the missing continuum data on the IW node. The required data include the particle velocity vector $\boldsymbol{u}_\mathrm{p}$ and the particle temperature T_p and is given by the time average over the last N microscopic steps and space average in an IW cell. With this substitute, central differencing can be employed to estimate derivatives in the direction normal to the interface (see figure 2). Regular central differencing is employed for derivatives in the direction parallel to the interface.

(*b*) *Flux boundary conditions on the continuum equations*

When the particle updates have been completed, equations (3.1)–(3.3) are updated by integrating the continuum equations (3.1)–(3.3) forward in time by the MacCormack predictor–corrector algorithm as is described by Anderson (1995). A time-step of $\Delta t = N\delta t = 1.0^{-13}$ s was used. In a first pass, flux densities were computed on all nodes, and predictions for the density, momentum and energy were made on each node according to the continuum equations. In a second pass, the flux densities were re-computed based on the predictions, and their values re-computed as a mean of the prediction and the correction.

The passes were carried out on an auxiliary lattice of twice the original resolution, i.e. half the original lattice spacing a, as is illustrated in figure 3. This is necessary due to the repeated use of centred differencing, in both the computation of fluxes and the subsequent computation of flux divergences.

To begin with, each original node projected its set of continuum values (mass density, velocity and temperature) onto four auxiliary nodes. The values on the set of IW auxiliary nodes were supplied by the corresponding averages of particle values.

First the continuum fluxes were computed according to equations (2.1)–(2.3). On the bulk auxiliary nodes and on the OW auxiliary nodes (nodes $\mathrm{OW_A}$ and $\mathrm{OW_C}$ in figure 3), derivatives of velocity and temperature were approximated using centred differencing.

On the outermost OW auxiliary nodes (nodes $\mathrm{OW_B}$ and $\mathrm{OW_D}$ in figure 3) and on the IW auxiliary nodes, the fluxes were not calculated; instead, the mean fluxes $\langle \boldsymbol{j} \rangle$, $\langle \boldsymbol{\Pi} \rangle$ and $\langle \boldsymbol{e} \rangle$ were inserted. The flux divergences were then computed on all the auxiliary nodes, using centred differencing everywhere. Again, on the edge nodes of the IW the computation was not possible. However, it was not needed since these nodes were used only to impose the boundary flux. Based on the flux divergences, the continuum equations were then integrated forward in time according to equations (3.1)–(3.3).

In the final step, the auxiliary lattice was reduced to the original lattice by taking averages of the auxiliary node values. To provide updated flux boundary conditions for the particles during the next N microscopic steps, the continuum fluxes were once again evaluated on the original lattice using the new continuum values, while substituting particle data for the missing continuum data on the IW nodes. As described in § 3 *a*, the resulting 'hybrid gradients' affected the continuum flux estimates and thus the mean fluxes found in the subsequent steps.

4. Imposing fluxes onto the particle system

(*a*) *Mass*

Imposing mass flux at the boundary of the particle domain means adding or removing particles. The normal component of the mean flux density, $a\langle \boldsymbol{j} \rangle \cdot \boldsymbol{n}$, is integrated over time. When the magnitude of the integrated flux exceeds half a particle mass m_p, a new particle is added, or an existing particle is removed.

A new particle is placed at a random position in the OW section of the particle domain. The position is chosen so that the new particle is separated from all existing particles by a minimum distance comparable with σ, the characteristic length of the interaction potential V_LJ. The initial velocity is zero.

To make the particle insertion as smooth as possible, the new particle initially does not interact with the existing particles. The interaction strength is increased gradually by a constant factor of 1.01, while the interaction forces experienced by the new particle remain below a threshold value. If the initial position is well chosen, the new particle reaches the strength of a regular particle within a few time-steps.

To remove a particle, the particle within the OW section that is closest to the domain boundary is identified. Its interaction strength is slowly reduced during subsequent MD steps. When the strength is zero, the particle is removed from the list of regular particles.

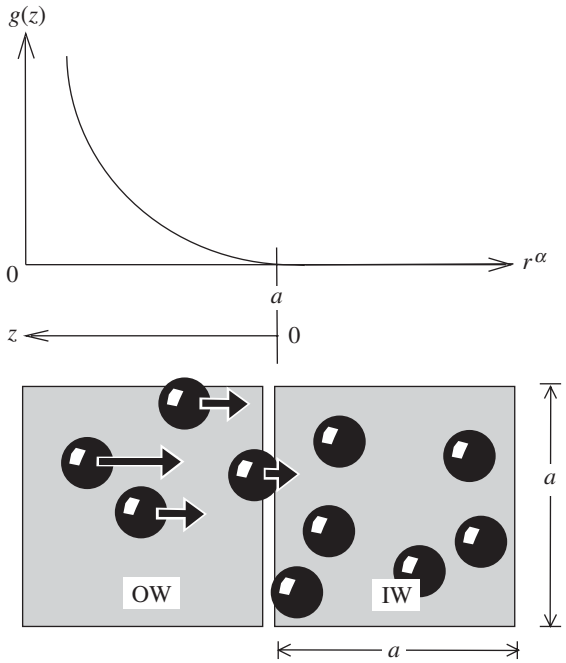

Figure 4. Schematic of the weight function $g(z)$.

The particle addition-and-removal procedure is designed not to cause changes of momentum and energy. The energy and momentum changes due to varying a particle's interaction strength are evaluated and registered. The change of the potential and kinetic energy of the particles is compensated by re-scaling the velocities of the regular neighbouring particles. The momentum change is likewise compensated by accelerating the neighbouring particles. These adjustments employ the same mechanisms that are used to impose energy and momentum flux onto the particles in the OW section: see below.

(*b*) *Momentum*

The normal component of the momentum flux density tensor, integrated across a sector length a, represents a stress force $\boldsymbol{F}_{\Pi} = \boldsymbol{n} \cdot \langle \boldsymbol{\Pi} \rangle a$. In order to localize the particles in the OW section, $\boldsymbol{F}_{\Pi}$ is applied in a non-homogeneous fashion, i.e.

$$\boldsymbol{F}_{\Pi}^{i} = \frac{g(z^i)}{\sum_{j \in V} g(z^j)} \boldsymbol{F}_{\Pi}, \tag{4.1}$$

where the normalizing sum is taken over all particles in the OW section of size a^2 and we have introduced an ad hoc distribution function $g(z)$ of zero magnitude and slope at the OW–IW section boundary, and of infinite magnitude at the domain boundary (see figure 4). The coordinate z is oriented toward the domain boundary and perpendicular to the interface, and its origin is located at the edge of the OW section. It is defined as

$$g(z) = \frac{1}{a - z} - \frac{1}{a} - \frac{z}{a^2} \quad \text{for } 0 \leqslant z \leqslant a.$$

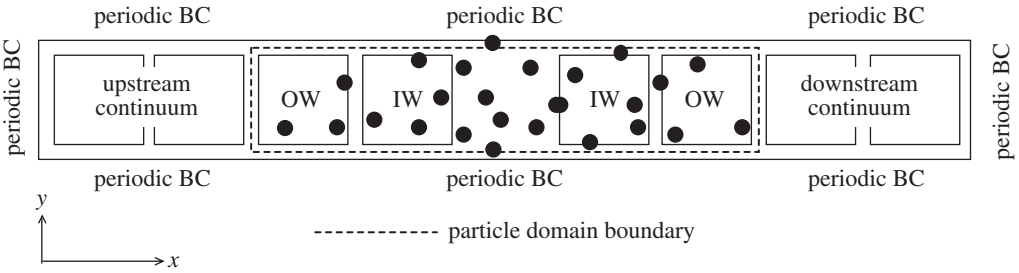

Figure 5. Schematic of the set-up used in periodic flow.

(c) *Energy*

The energy of the particle system must be adjusted to account for energy influx and outflux. In a sector of length a, the energy change δE due to flux during a microscopic step is

$$\delta E = \overline{e^{\alpha}} a \delta t. \tag{4.2}$$

The same amount of excess energy is assigned to each of N_{OW} particles, i.e.

$$\delta E^i = \frac{\delta E}{N_{\mathrm{OW}}}. \tag{4.3}$$

In addition, adjustment is required to compensate for energy changes due to particle creation and absorption, and for the action of stress forces. The adjustment must take place without changing the total momentum of the particles system. In each microscopic step, the thermal velocities of particles in the OW section are *re-scaled* according to

$$(\boldsymbol{u}^i - \boldsymbol{u}_0) \to \sqrt{1 + \frac{\Delta E}{\sum_{j \in V} E^j_{\mathrm{therm}}}} (\boldsymbol{u}^i - \boldsymbol{u}_0), \tag{4.4}$$

where the sum is taken over all N_{OW} particles, $\boldsymbol{u}_0$ is the averaged velocity in OW, $E^j_{\mathrm{therm}} = \frac{1}{2} m_{\mathrm{p}} (\boldsymbol{u}^i - \boldsymbol{u}_0)^2$ is the thermal energy of the jth particle, and ΔE is the energy quantum to be added. The total momentum is conserved in this operation.

5. Application to homogeneous flow in a periodic system

In order to test the scheme, a particle domain was set between two continuum domains that were connected by periodic boundary conditions (see figure 5). The simulation began with a relaxation stage during which the particles were kept at constant temperature. The flux coupling was activated only after a given number of relaxation steps had been completed. A rectangular node lattice of spacing $2a \times a$, with the longer dimension perpendicular to the particle-continuum interface, was used. The continuum was represented by $n \times 1$ nodes, and the particle domain had a size of $m \times 1$ nodes. Four nodes were used for the overlap region and represented the upstream and downstream OW and IW sections. Periodic boundary conditions were applied in the x- and y-directions.

At the end of the relaxation stage, the mass density and temperature in the particle domain differed from the corresponding values in the continuum domain. Figure 6 shows that the values adjusted in the course of the simulation. This adjustment is the

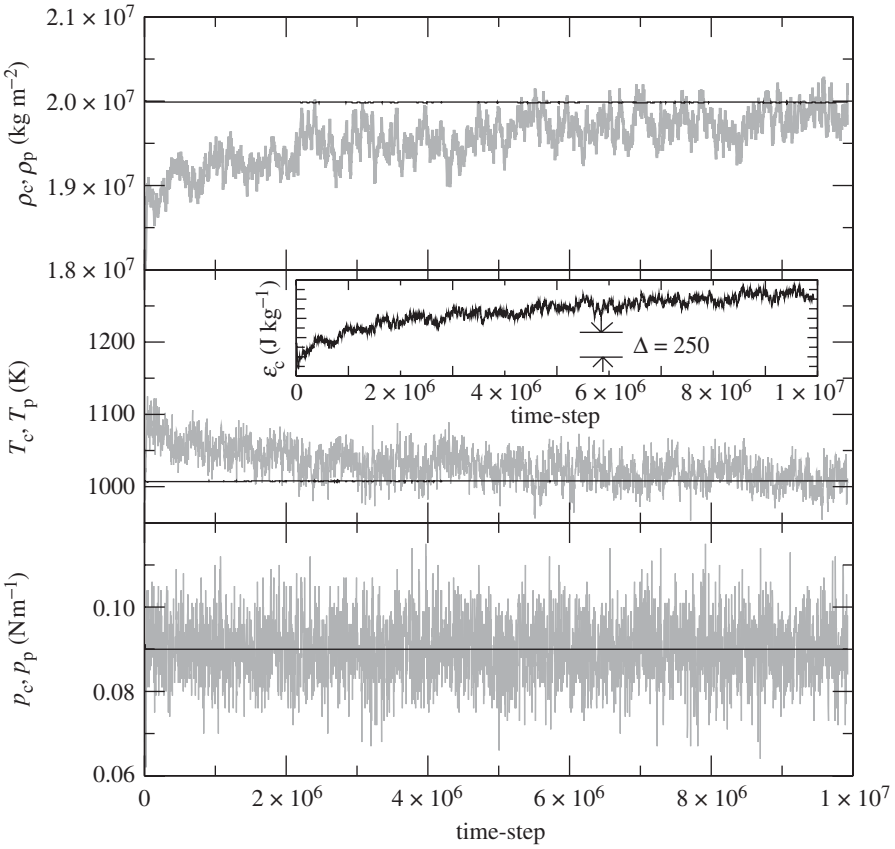

Figure 6. Plot of mass density ρ, temperature T and pressure p measured during the equilibration phase. The particle data are shown by the fluctuating grey lines and the continuum by the black lines. The inset shows the continuum energy per unit mass, ϵ_c.

direct consequence of the use of hybrid gradients in the computation of continuum fluxes. The continuum values appear constant on the scale of the plots due to the large continuum mass. However, in the inset, ϵ_c is observed to adjust. Note that the pressure values p_c and p_p match throughout the simulation, since these enter directly into the flux-exchange scheme.

To study flow across the continuum–particle interface, a simulation was started as described above. After 5×10^5 microscopic time-steps, a body force acted temporarily in the positive x-direction. Then the body force was switched off, steady-state flow was reached, with particles being created at the upstream interface and absorbed at the downstream interface about every 100 time-steps.

The acceleration and subsequent steady-flow stages are reflected in figure 7, which shows the spatial averages of the continuum and the particle data for the mass m, the momentum P in the flow direction, and the total energy E. The insets show the total mass, momentum and energy during the steady-flow stage on a finer scale.

This simulation is a stringent test of conservation of mass, momentum and energy, showing the distribution of these quantities due to fluctuations as well as adherence to the overall conservation laws.

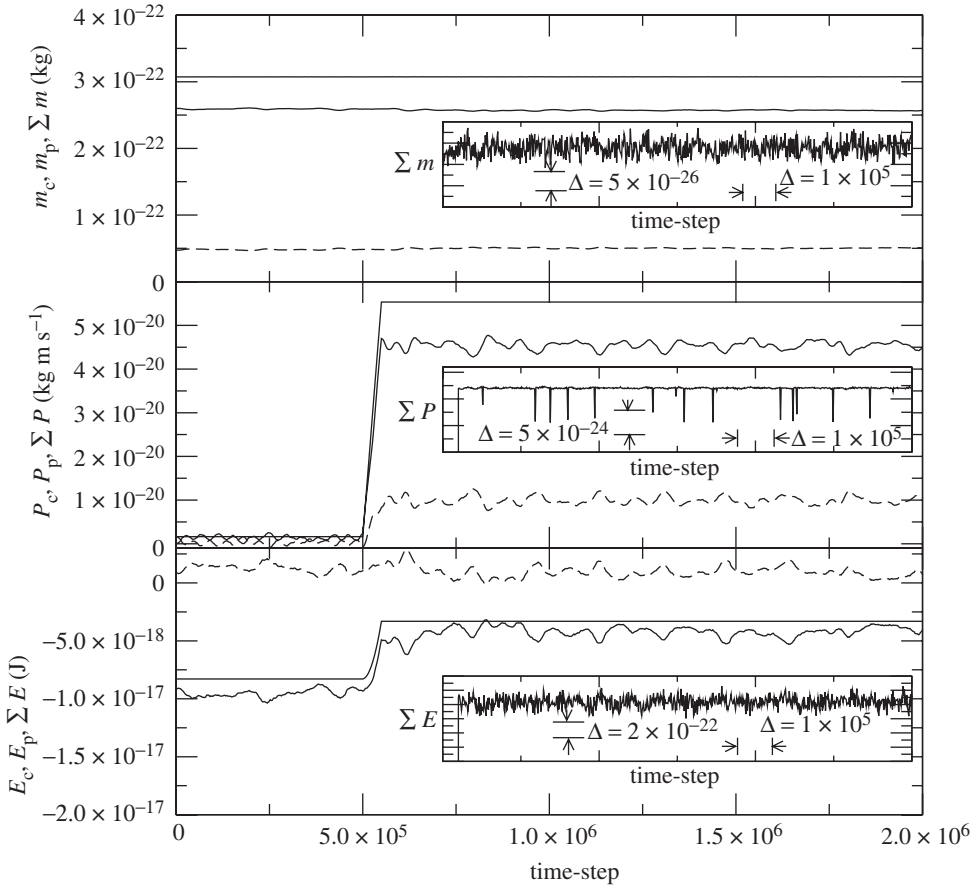

Figure 7. Plot of mass m, momentum P and total energy E measured during a study of flow in a periodic system. Solid lines refer to the continuum, dashed lines to the particle domain and bold lines to the entire system. The insets additionally show the total sums, but on a finer scale.

During the steady-state stage, the combined sums of particle and continuum mass, momentum and total energy appear constant on the scale of the plots; inspection reveals that the systematic deviations due to drifts were only of relative order 10^{-4}.

6. Discussion

Flux-exchange schemes have been applied in the context of dilute gases (see Garcia *et al*. 1999; Roveda *et al*. 1998, 2000), and in problems of simple diffusion (Plapp & Karma 2000; Flekkøy *et al*. 2001). In the present scheme, flux exchange is used to couple particles and continuum in a symmetric and consistent fashion for a *dense fluid system*. An important feature of our flux-exchange scheme is the use of *hybrid gradients* in the computation of continuum fluxes at the boundary of the continuum domain. This is the case also in the related work of by Delgado-Buscalioni & Coveney (2003). As pointed out above, this feature is necessary to achieve thermal equilibrium even in the absence of advective flow.

In preliminary tests, we have used a coupling scheme in which no hybrid gradients were taken; instead, the continuum gradients in the OW section were approximated by forward or backward differencing, involving differences with respect to the adjacent bulk continuum nodes only. In such a scheme the pressure in the coupled domains is still found to match, but temperature does not adjust in the absence of advective flow.

The observed conservation of mass, momentum and energy is not trivially achieved, as the construction of the coupling scheme may appear to indicate. If the particle system is out of thermal equilibrium, the upstream and downstream OW sections will become either depleted of particles or crammed with particles. In the first case, momentum and energy cannot be transmitted onto the particles and conservation is violated. In the second case, leakage of particles will abound and particle re-insertion will mostly fail, so that mass is not conserved. If thermal equilibrium is maintained, as in the present case, systematic energy drift due to overly strong perturbation of particle trajectories in the OW sections is difficult to avoid. The present extremely small drift is the result of careful tuning of the particle-insertion and particle-removal mechanisms. It is assumed that the scheme will become more robust by the design of more stable particle flux boundary conditions.

We gratefully acknowledge helpful discussions with J. Adler, A. Aharony, I. Goldhirsch, and O. Entin-Wohlmann. We thank S. Brandon for useful comments and for permission to use computer resources. G.W. was partially supported by Tel Aviv University and by Schweizerischer Nationalfonds. In the final stage of this work, the hospitality of the Computational Physics Group at the Technion Israel Institute of Technology was highly appreciated. This research was also supported by the research contract 462000-98/0 between Norsk Hydro ASA and Fracton AS.

References

Abraham, F. F., Broughton, J. Q., Bernstein, N. & Kaxiras, E. 1998 *Computers Phys.* **12**, 538.

Anderson, D. A. 1995 *Computational fluid dynamics*. McGraw-Hill.

Delgado-Buscalioni, R. & Coveney, P. V. 2003 *Phys. Rev.* E **67**, 046704.

Flekkøy, E. G., Wagner, G. & Feder, J. G. 2000 *Europhys. Lett.* **52**, 271.

Flekkøy, E. G., Feder, J. G. & Wagner, G. 2001 *Phys. Rev.* E **64**, 066302.

Garcia, A. L., Bell, J. B., Crutchfield, W. Y. & Alder, B. J. 1999 *J. Comput. Phys.* **154**, 134.

Hadjiconstantinou, N. G. 1999*a* *Phys. Rev.* E **59**, 2475.

Hadjiconstantinou, N. G. 1999*b* *J. Comput. Phys.* **154**, 245.

O'Connel, S. T. & Thompson, P. A. 1995 *Phys. Rev.* E **52**, 5792.

Plapp, M. & Karma, A. 2000 *Phys. Rev. Lett.* **84**, 1740.

Rafii, H., Hua, L. & Cross, M. 1998 *J. Phys. Condens. Matter* **10**, 2375.

Resibois, P. & De Leener, M. 1977 *Classical kinetic theory of fluids*. Wiley.

Roveda, R., Goldstein, D. & Varghese, P. 1998 *J. Spacecraft Rockets* **35**, 258.

Roveda, R., Goldstein, D. & Varghese, P. 2000 Hybrid Euler/direct simulation Monte Carlo calculation of unsteady slit flow. *J. Spacecraft Rockets* **37**, 753.

Wagner, G., Flekkøy, E. G., Feder, J. G. & Jøssang, T. F. 2002 *Comput. Phys. Commun.* **147**, 670.